

NUMERICAL SIMULATION OF UNSTEADY COMPRESSIBLE LOW MACH NUMBER FLOW IN A CHANNEL

Petra Punčochářová-Pořízková*, Karel Kozel**, Jaromír Horáček**, Jiří Fürst*

This study deals with the numerical solution of a 2D unsteady flow of a compressible viscous fluid in a channel for low inlet airflow velocity. The unsteadiness of the flow is caused by a prescribed periodic motion of a part of the channel wall with large amplitudes, nearly closing the channel during oscillations. The channel is a simplified model of the glottal space in the human vocal tract and the flow can represent a model of airflow coming from the trachea, through the glottal region with periodically vibrating vocal folds to the human vocal tract.

The flow is described by the system of Navier-Stokes equations for laminar flows. The numerical solution is implemented using the finite volume method (FVM) and the predictor-corrector MacCormack scheme with Jameson artificial viscosity using a grid of quadrilateral cells. Due to the motion of the grid, the basic system of conservation laws is considered in the Arbitrary Lagrangian-Eulerian (ALE) form.

The authors present the numerical simulations of flow fields in the channel, acquired from a program developed exclusively for this purpose. The numerical results for unsteady flows in the channel are presented for inlet Mach number $M_\infty = 0.012$, Reynolds number $Re_\infty = 5 \times 10^3$ and the wall motion frequency 100 Hz.

Keywords: CFD, Finite Volume Method, unsteady flow, low Mach number, viscous compressible fluid

1. Introduction

Fluid-structure interaction problems can be treated in numerous engineering and other applications. This study presents a numerical solution of compressible viscous flows in a channel that represents a model of glottal spaces in the human vocal tract.

In current publications such flow models are mostly based on the Bernoulli equation [1] or 1D models for an incompressible inviscid fluid [2]. Acoustic wave propagation in the vocal tract is usually modeled separately using linear acoustic perturbation theory, the wave equation for the potential flow [3] or the Lighthill approach on sound generated aerodynamically [4]. A current challenging question is a mathematical and physical description of the mechanism for transforming the airflow energy in the glottis into the acoustic energy representing the voice source in humans. The voice source signal travels from the glottis to the mouth, exciting the acoustic supraglottal spaces, and becomes modified by acoustic resonance properties of the vocal tract [1]. Also, it is not clear so far how to model

* Ing. P. Punčochářová-Pořízková, Ph.D., doc. Ing. J. Fürst, Ph.D., Dept. of Technical Mathematics, FME CTU, Karlovo nám. 13, 121 35 Praha 2, Czech Republic

** prof. RNDr. K. Kozel, DrSc., Ing. J. Horáček, DrSc., Institute of Thermomechanics AS CR, Dolejškova 5, Prague 8, Czech Republic

the separation point on a moving surface in a small gap. This is usually approximated by quasi-steady formulas deduced from steady flow solutions in divergent channels [5], yet the validity of this procedure for higher frequencies is questionable. The airflow in the glottis described by the 2D Navier-Stokes equations for an incompressible laminar flow was studied in [6] using FVM and in [7] using Finite Element Method (FEM). FIDAP software was used in [8] for 3D modeling of the flow in the glottis by FEM using the Navier-Stokes equations for an incompressible fluid.

The authors present a flow model based on the Navier-Stokes equations for a compressible viscous fluid. In reality, the airflow coming from the lungs causes self-oscillations of the vocal folds, and the glottis completely closes in normal phonation regimes, generating acoustic pressure fluctuations. In this study, the periodic changes of the channel cross-section are prescribed; the channel is harmonically opening and nearly closing in the narrowest cross-section of the channel as a first approximation of reality, making the investigation of the airflow field in the glottal region possible. A mathematical model of a compressible viscous fluid is used because when the glottis is closing, the local airflow velocity reaches quite high values in the narrowest part of the airways and where the viscous forces are important as well. For an inviscid incompressible flow, the maximum flow velocity would be very high (tends to infinity) just before the glottis closes. For phonation of vowels, the airflow volume velocity in the vocal tract is in the range $0.07\text{--}0.85\text{ m s}^{-1}$ i.e. the airflow velocity in the trachea approximately in the range of $0.3\text{--}5.2\text{ m s}^{-1}$ taking into account the tracheal diameter in humans in the range $14.5\text{--}17.6\text{ mm}$ [3]. In this numerical simulation, a uniform inflow Mach number $M_\infty = 0.012$ (air velocity 4.12 m s^{-1}) is assumed. Particular attention is paid to the analysis of the position of the flow separation point on the vibrating surface, and to the interrelations between the flow velocity, flow rate and pressure waveforms and the motion of the oscillating glottal orifice.

2. Mathematical model

To describe the unsteady laminar flow of a compressible viscous fluid in a channel, the 2D system of Navier-Stokes equations was considered as a mathematical model. The Navier-Stokes equations were transformed to non-dimensional form. The transformation of dimensional variables (marked with the accent hat) to non-dimensional variables is defined as follows:

$$\begin{aligned} \rho &\rightarrow \frac{\hat{\rho}}{\hat{\rho}_\infty}, & (u, v) &\rightarrow \frac{(\hat{u}, \hat{v})}{\hat{c}_\infty}, & (x, y) &\rightarrow \frac{(\hat{x}, \hat{y})}{\hat{L}_r}, & t &\rightarrow \frac{\hat{t}\hat{c}_\infty}{\hat{L}_r}, \\ p &\rightarrow \frac{\hat{p}}{\hat{\rho}_\infty \hat{c}_\infty^2}, & e &\rightarrow \frac{\hat{e}}{\hat{\rho}_\infty \hat{c}_\infty^2}, & \eta &\rightarrow \frac{\hat{\eta}}{\hat{\eta}_\infty}, & T &\rightarrow \frac{\hat{T}}{\hat{T}_\infty}, \end{aligned} \quad (1)$$

where ρ denotes density, u and v are the components of the velocity vector, p denotes pressure and e is the total energy per unit volume. The reference variables in this case are inflow variables (marked with the infinity subscript): the speed of sound $\hat{c}_\infty = 343\text{ ms}^{-1}$, density $\hat{\rho}_\infty = 1.225\text{ kg m}^{-3}$, temperature $\hat{T}_\infty = 293.15\text{ K}$, dynamic viscosity $\hat{\eta}_\infty = 15 \times 10^{-6}\text{ Pa s}$ and a reference length $\hat{L}_r = 0.02\text{ m}$. The system of Navier-Stokes equations is expressed in non-dimensional conservative form [9] as:

$$\frac{\partial \mathbf{W}}{\partial t} + \frac{\partial \mathbf{F}}{\partial x} + \frac{\partial \mathbf{G}}{\partial y} = \frac{1}{Re} \left(\frac{\partial \mathbf{R}}{\partial x} + \frac{\partial \mathbf{S}}{\partial y} \right), \quad (2)$$

where

$$\mathbf{W} = [\rho, \rho u, \rho v, e]^T, \quad (3)$$

$$\mathbf{F} = [\rho u, \rho u^2 + p, \rho u v, (e + p) u]^T, \quad (4)$$

$$\mathbf{G} = [\rho v, \rho u v, \rho v^2 + p, (e + p) v]^T, \quad (5)$$

$$\mathbf{R} = \begin{pmatrix} 0 \\ \frac{2}{3} \eta \left(2 \frac{\partial u}{\partial x} - \frac{\partial v}{\partial y} \right) \\ \eta \left(\frac{\partial u}{\partial y} + \frac{\partial v}{\partial x} \right) \\ \frac{2}{3} \eta \left(2 \frac{\partial u}{\partial x} - \frac{\partial v}{\partial y} \right) u + \eta \left(\frac{\partial u}{\partial y} + \frac{\partial v}{\partial x} \right) v + k \frac{\partial T}{\partial x} \end{pmatrix}, \quad (6)$$

$$\mathbf{S} = \begin{pmatrix} 0 \\ \eta \left(\frac{\partial u}{\partial y} + \frac{\partial v}{\partial x} \right) \\ \frac{2}{3} \eta \left(-\frac{\partial u}{\partial x} + 2 \frac{\partial v}{\partial y} \right) \\ \eta \left(\frac{\partial u}{\partial y} + \frac{\partial v}{\partial x} \right) u + \frac{2}{3} \eta \left(-\frac{\partial u}{\partial x} + 2 \frac{\partial v}{\partial y} \right) v + k \frac{\partial T}{\partial y} \end{pmatrix}, \quad (7)$$

\mathbf{W} is the vector of conservative variables, \mathbf{F} and \mathbf{G} are the vectors of inviscid fluxes, \mathbf{R} and \mathbf{S} are the vectors of viscous fluxes. General Reynolds number in (2) is computed from reference variables $Re = \hat{\rho}_\infty \hat{c}_\infty \hat{L}_r / \hat{\eta}_\infty$. The static pressure p is expressed by the state equation in the form

$$p = (\kappa - 1) \left[e - \frac{1}{2} \rho (u^2 + v^2) \right]. \quad (8)$$

The non-dimensional dynamic viscosity in the dissipative terms (6) and (7) is a function of temperature in the form $\eta = (T/T_\infty)^{3/4}$. The heat transfer coefficient is expressed as $k = \eta \kappa / [Pr(\kappa - 1)]$, where $Pr = 0.7$ is the Prandtl number and $\kappa = 1.4$ is the ratio of the specific heats (the Poisson coefficient).

3. Computational domain and boundary conditions

The bounded computational domain D , used for the numerical solution of flow field in the channel, is shown in Figure 1. The domain is a symmetric channel, the shape of which is inspired by the shape [10] of the trachea (inlet part of the channel), vocal folds, false vocal folds and supraglottal spaces (outlet part). The upper and the lower boundaries are the channel walls. A part of the wall changes its shape between the points A and B according to a given function of time and axial coordinate:

$$\begin{aligned} w(x, t) &= (a_1 + a_t) \left[\sin \left\{ \frac{3\pi}{2} + \pi \frac{x - x_A}{x_C - x_A} \right\} + 1 \right] + d, \quad x \in \langle x_A, x_C \rangle, \\ w(x, t) &= 2(a_1 + a_t) \cos \left(\frac{\pi}{2} \frac{x - x_C}{x_B - x_C} \right) + d, \quad x \in (x_C, x_B), \\ a_t &= a_2 \sin(2\pi f t), \quad t \in \langle 0, 2\pi \rangle, \end{aligned} \quad (9)$$

where $f = 5.83 \times 10^{-3}$ is the dimensionless frequency, which corresponds to the real frequency 100 Hz, typical for normal male voice. Base amplitude $a_1 = 0.18$ (3.6 mm) and amplitude of time oscillation $a_2 = 0.015$ (0.3 mm) are set according to maximum and minimum gap. The gap $g = 2 \{(d + h) - w(x_C, t)\}$ is the narrowest part of the channel (in point C).

The considered dimensions of the domain are summarized in Table 1. The gap width was oscillating between the minimum $g_{\min} = 0.4$ mm and maximum $g_{\max} = 2.8$ mm, not closing the channel completely.

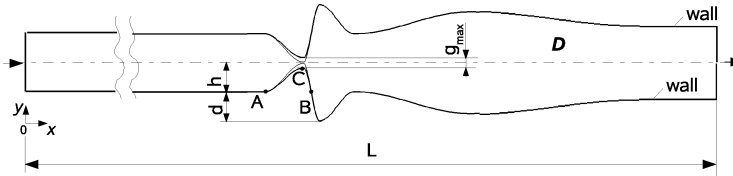


Fig.1: Computational domain D

	x [–]	y [–]	\hat{x} [mm]	\hat{y} [mm]
A	9.75	0.4	195	8
B	10.4	0	208	0
C	10.3	$w(x_C, t)$	206	$w(x_C, t) \cdot 20$
g_{\min}	—	0.02	—	0.4
g_{\max}	—	0.14	—	2.8
L	16	—	320	—
h	—	0.4	—	8
d	—	0.4	—	8

Tab.1: Dimensions of computational domain D

The boundary conditions are considered in the following formulation:

1. Upstream conditions: $u_\infty = M_\infty \cos(\alpha) = M_\infty$, $v_\infty = M_\infty \sin(\alpha) = 0$, $\rho_\infty = 1$, p_∞ is extrapolated from domain D and $\alpha = 0$ is the angle of the incoming flow.
2. Downstream conditions: $p_2 = 1/\kappa$, $(\rho, \rho u, \rho v)$ are extrapolated from D .
3. Flow on the wall: $(u, v) = (u_{\text{wall}}, v_{\text{wall}})$ and $\frac{\partial T}{\partial n} = 0$. ($T = \kappa p/\rho$ is the temperature).

If the problem with the boundary conditions is related to known values of the inlet velocity and length, than the real flow field is simulated and the Reynolds number at the inlet is computed from the inflow variables $Re_\infty = \hat{\rho}_\infty \hat{u}_\infty \hat{H}/\hat{\eta}_\infty$, where $\hat{H} = 2h\hat{L}_r$ is the inflow width of the channel (see Figure 1) and $\hat{u}_\infty = M_\infty \hat{c}_\infty$ is inflow air-velocity. Than the general Reynolds number is $Re = Re_\infty$.

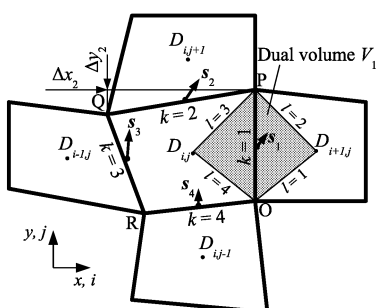


Fig.2: Finite volume $D_{i,j}$ and dual volume V'_k

4. Numerical solution

The numerical solution uses FVM in conservative cell-centered form on the grid of quadrilateral cells, see e.g. [9].

The bounded domain is divided into mutually disjoint sub-domains $D_{i,j}$ (i.e. quadrilateral cells). The system of equations (2) is integrated over the sub-domains $D_{i,j}$ using the Green formula and the Mean value theorem. In the time-changing domain, the integral form of FVM is derived using the ALE

formulation. The ALE method defines homeomorphic mapping of the reference domain $D_{t=0}$ at initial time $t = 0$ to a domain D_t at $t > 0$ [11].

The explicit predictor-corrector MacCormack (MC) scheme in the domain with a moving grid of quadrilateral cells is used. The scheme is 2nd order accurate in time and space [9] :

$$\begin{aligned} \mathbf{W}_{i,j}^{n+1/2} &= \frac{\mu_{i,j}^n}{\mu_{i,j}^{n+1}} \mathbf{W}_{i,j}^n - \frac{\Delta t}{\mu_{i,j}^{n+1}} \sum_{k=1}^4 \left[\left(\tilde{\mathbf{F}}_k^n - s_{1k} \mathbf{W}_k^n - \frac{1}{Re} \tilde{\mathbf{R}}_k^n \right) \Delta y_k - \right. \\ &\quad \left. - \left(\tilde{\mathbf{G}}_k^n - s_{2k} \mathbf{W}_k^n - \frac{1}{Re} \tilde{\mathbf{S}}_k^n \right) \Delta x_k \right], \\ \overline{\mathbf{W}}_{i,j}^{n+1} &= \frac{\mu_{i,j}^n}{\mu_{i,j}^{n+1}} \frac{1}{2} \left(\mathbf{W}_{i,j}^n + \mathbf{W}_{i,j}^{n+1/2} \right) - \\ &\quad - \frac{\Delta t}{2 \mu_{i,j}^{n+1}} \sum_{k=1}^4 \left[\left(\tilde{\mathbf{F}}_k^{n+1/2} - s_{1k} \mathbf{W}_k^{n+1/2} - \frac{1}{Re} \tilde{\mathbf{R}}_k^{n+1/2} \right) \Delta y_k - \right. \\ &\quad \left. - \left(\tilde{\mathbf{G}}_k^{n+1/2} - s_{2k} \mathbf{W}_k^{n+1/2} - \frac{1}{Re} \tilde{\mathbf{S}}_k^{n+1/2} \right) \Delta x_k \right], \end{aligned} \quad (10)$$

where $\Delta t = t^{n+1} - t^n$ is the time step, $\mu_{i,j} = \iint_{D_{i,j}} dx dy$ is the volume of cell $D_{i,j}$, Δx and Δy are the steps of the grid in directions x and y , vector $\mathbf{s}_k = (s_1, s_2)_k$ represents the speed of edge k (see Figure 2). The physical fluxes $\mathbf{F}, \mathbf{G}, \mathbf{R}, \mathbf{S}$ on the edge k of the cell $D_{i,j}$ are replaced by numerical fluxes (marked with tilde) $\tilde{\mathbf{F}}, \tilde{\mathbf{G}}, \tilde{\mathbf{R}}, \tilde{\mathbf{S}}$ as approximations of the physical fluxes.

The approximations of the convective terms $\mathbf{s} \mathbf{W}_k$ and the numerical viscous fluxes $\tilde{\mathbf{R}}_k, \tilde{\mathbf{S}}_k$ on the edge k are central. The higher partial derivatives of velocity and temperature in $\tilde{\mathbf{R}}_k, \tilde{\mathbf{S}}_k$ are approximated using dual volumes V'_k (see [9]) as shown in Figure 2. The inviscid numerical fluxes are approximated by the physical fluxes from the cell on the left side of the current edge in the predictor step and from the cell on the right side of the current edge in the corrector step.

The last term used in the MC scheme is the Jameson artificial dissipation [12] :

$$\begin{aligned} AD(W_{i,j})^n &= C_1 \gamma_1 (\mathbf{W}_{i+1,j}^n - 2 \mathbf{W}_{i,j}^n + \mathbf{W}_{i-1,j}^n) + \\ &\quad + C_2 \gamma_2 (\mathbf{W}_{i,j+1}^n - 2 \mathbf{W}_{i,j}^n + \mathbf{W}_{i,j-1}^n), \end{aligned} \quad (11)$$

where $C_1, C_2 \in R$ are constants, in our case $C_1 = 1.7$, $C_2 = 1.5$, and the variables γ_1, γ_2 have the form :

$$\gamma_1 = \frac{|p_{i+1,j}^n - 2p_{i,j}^n + p_{i-1,j}^n|}{|p_{i+1,j}^n| + 2|p_{i,j}^n| + |p_{i-1,j}^n|}, \quad \gamma_2 = \frac{|p_{i,j+1}^n - 2p_{i,j}^n + p_{i,j-1}^n|}{|p_{i,j+1}^n| + 2|p_{i,j}^n| + |p_{i,j-1}^n|}. \quad (12)$$

Since the artificial dissipation term is of third order, the overall accuracy of the scheme is of second order. The vector of conservative variables \mathbf{W} can be computed at a new time level t^{n+1} :

$$\mathbf{W}_{i,j}^{n+1} = \overline{\mathbf{W}}_{i,j}^{n+1} + AD(W_{i,j})^n. \quad (13)$$

The stability condition of the scheme (on the regular orthogonal grid) limits the time step :

$$\Delta t \leq CFL \left[\frac{|u_{\max}| + c}{\Delta x_{\min}} + \frac{|v_{\max}| + c}{\Delta y_{\min}} + \frac{2}{Re} \left(\frac{1}{\Delta x_{\min}^2} + \frac{1}{\Delta y_{\min}^2} \right) \right]^{-1}, \quad (14)$$

where c denotes the local speed of sound, u_{\max} and v_{\max} are the maximum velocities in the domain, and $CFL < 1$ for non-linear equations [13].

The grid used in the channel has successive refinement cells near the wall. The minimum cell size in y -direction is $\Delta y_{\min} \approx 1/\sqrt{Re}$ to capture the boundary layer effects. Figure 3 shows the detail of the grid in domain D in the narrowest channel cross-section at the middle position of the gap.

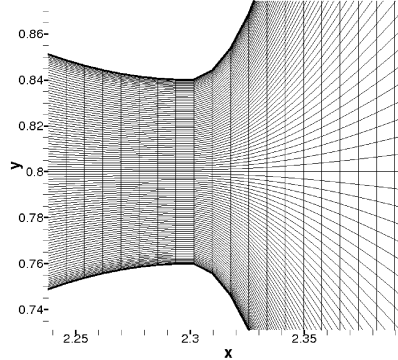


Fig.3: Grid of quadrilateral cells in part of domain D at the middle position of the gap width

5. Numerical results

The numerical results were obtained (using a specifically developed program) for the following input data: Mach number $M_{\infty} = 0.012$ ($\hat{u}_{\infty} = 4.116 \text{ m s}^{-1}$), Reynolds number $Re_{\infty} = 5378$, atmospheric pressure $p_2 = 1/\kappa$ ($\hat{p}_2 = 102942 \text{ Pa}$) at the outlet, and wall oscillation frequency $\hat{f} = 100 \text{ Hz}$. The computational domain contained 450×100 cells in D .

The computation has been carried out in two stages. First, a numerical solution is obtained, when the channel between points A and B has a rigid wall fixed in the middle position of the gap width. Then this solution is used as the initial condition for the unsteady simulation (see [14]).

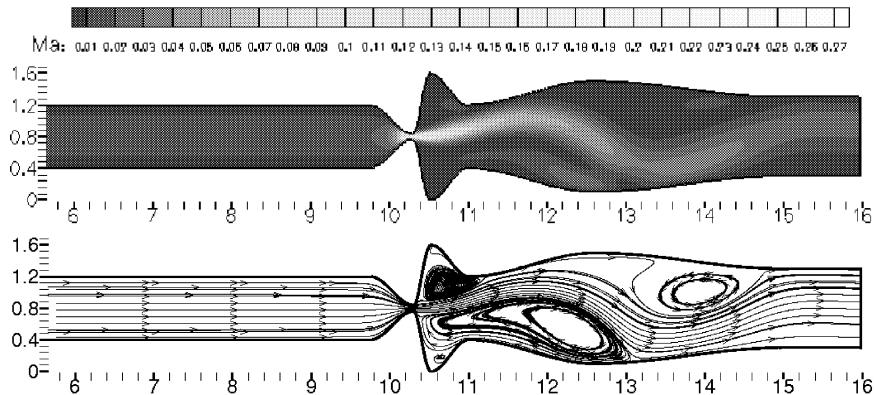
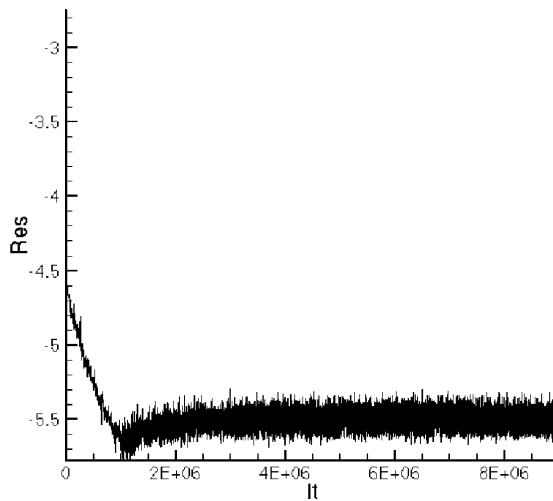


Fig.4: The initial condition; computed in $D - M_{\infty} = 0.012$, $Re_{\infty} = 5378$, $p_2 = 1/\kappa$, 450×100 cells, $M_{\max} = 0.190$; results are mapped by iso-lines of Mach number and streamlines (the inlet part of the channel is abridged)



*Fig.5: Convergence to the steady state solution – $M_\infty = 0.012$,
 $Re = 5378$, $p_2 = 1/\kappa$, 450×100 cells*

Figure 4 shows the initial condition for unsteady computation of the flow field in domain D . The maximum Mach number computed in the domain was $M_{\max} = 0.190$. The pictures display non-symmetric flow developed behind the narrowest channel cross-section. Figure 5 shows the convergence to the steady state solution computed using the L_2 norm of momentum residuals (ρu). The graph indicates the non-stationary solution which is caused probably by eddies separated in the unmoving glottal orifice and floating away.

The numerical simulation of the air-flow computed in domain D over the fourth cycle of the wall oscillation is presented in Figure 6 Part A, Part B, Part C showing the unsteady flow field in ten time instants during one vibration period. The chosen time instants (a)–(j) are marked in Figure 7. Large eddies are developing in supraglottal spaces and a ‘Coandă’ effect is apparent in the flow field pattern. The absolute maximum of Mach number $M = 0.270$ (corresponding to the dimension velocity 92.61 m s^{-1}) in the flow field during fourth cycle was achieved at time $t = 36.12 \text{ s}$ behind the narrowest channel cross-section (see Figure 6(g)).

Figure 8 shows the following dimensional quantities computed in real time in two selected points of the flow field: the prescribed oscillation of gap width, the pressure registered at the inlet, the absolute airflow velocity at the distance x_C on the channel axis and flow rate calculated in the narrowest channel cross-section (at x_C). The phase shift (time delay) between the minimum glottal gap and the maximum of velocity (Mach number) is 3.62 ms, and similarly, the time delays in the pressure fluctuations and flow rate are about 2.5 ms and 4.3 ms, respectively. The flow behavior is remarkably different during opening and closing phases of the gap. The small pressure disturbances and the local peaks seen on the flow velocity graphs are caused by separated vortices and by the oscillating jet direction (‘Coandă’ effect). The minimum of airflow velocity and flow rate corresponds to the minimal gap width due to a dominant effect of viscous fluid forces in a very narrow gap. The flow becomes practically periodic after the first period of oscillations.

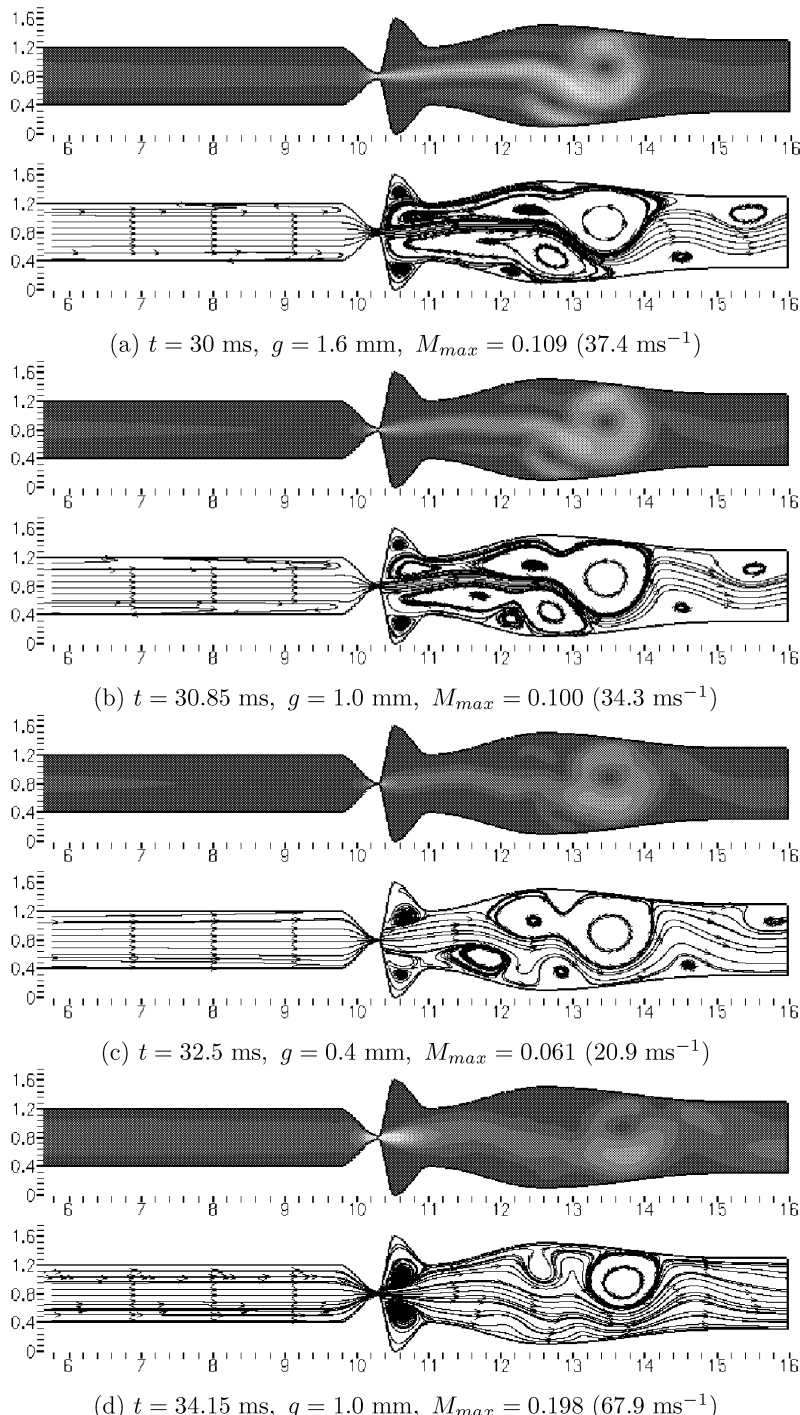


Fig.6: Part A – The unsteady numerical solution of the airflow in $D - \hat{f} = 100 \text{ Hz}$, $M_\infty = 0.012$, $Re_\infty = 5378$, $p_2 = 1/\kappa$, 450×100 cells; data computed during the fourth oscillation cycle; results are mapped by iso-lines of Mach number and by streamlines (the inlet part of the channel is abridged)

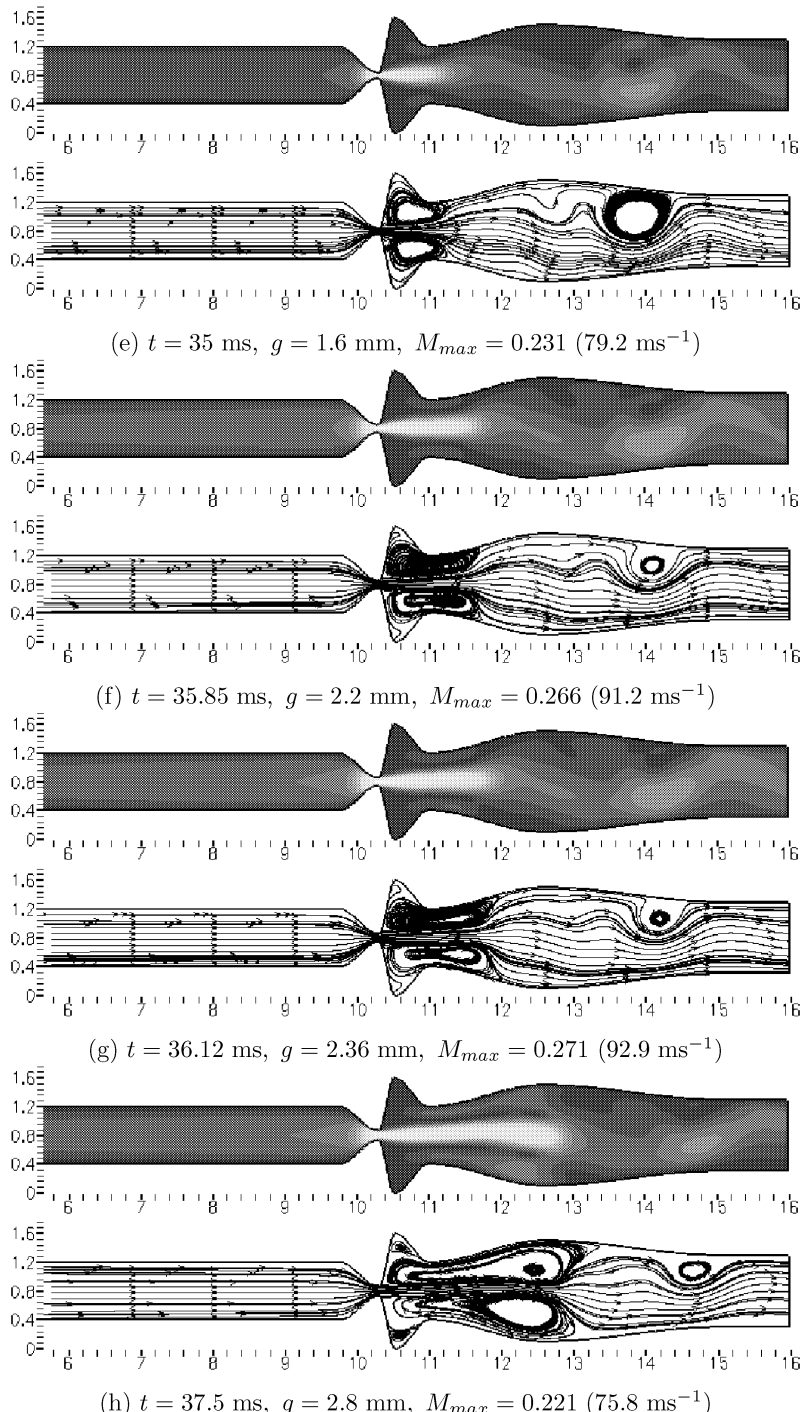
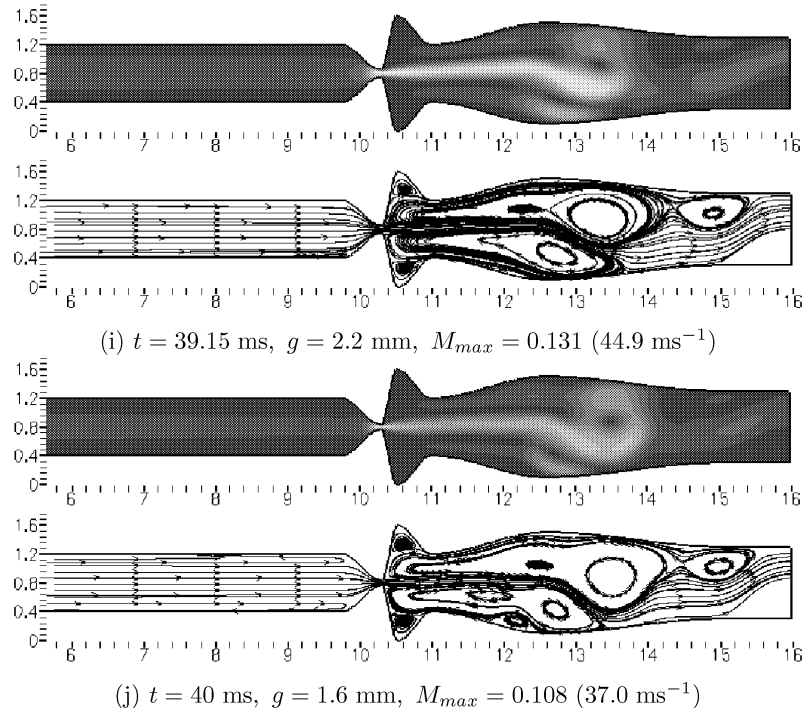


Fig.6: Part B – The unsteady numerical solution of the airflow in $D - \hat{f} = 100 \text{ Hz}$, $M_\infty = 0.012$, $Re_\infty = 5378$, $p_2 = 1/\kappa$, 450×100 cells; data computed during the fourth oscillation cycle; results are mapped by iso-lines of Mach number and by streamlines (the inlet part of the channel is abridged)



Ma: 0.01 0.02 0.03 0.04 0.05 0.06 0.07 0.08 0.09 0.1 0.11 0.12 0.13 0.14 0.15 0.16 0.17 0.18 0.19 0.2 0.21 0.22 0.23 0.24 0.25 0.26 0.27

Fig.6: Part C – The unsteady numerical solution of the airflow in D – $\hat{f} = 100 \text{ Hz}$, $M_\infty = 0.012$, $Re_\infty = 5378$, $p_2 = 1/\kappa$, 450×100 cells; data computed during the fourth oscillation cycle; results are mapped by iso-lines of Mach number and by streamlines (the inlet part of the channel is abridged)

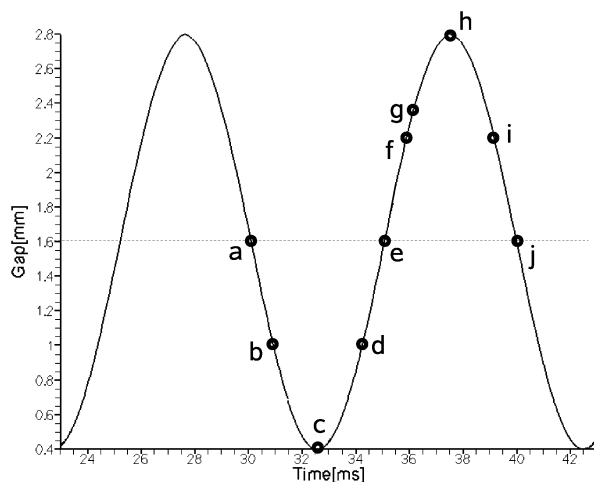


Fig.7: Time instants (a)–(j) for which the flow field patterns are presented in Fig. 6 during fourth period of the glottal gap oscillation cycle

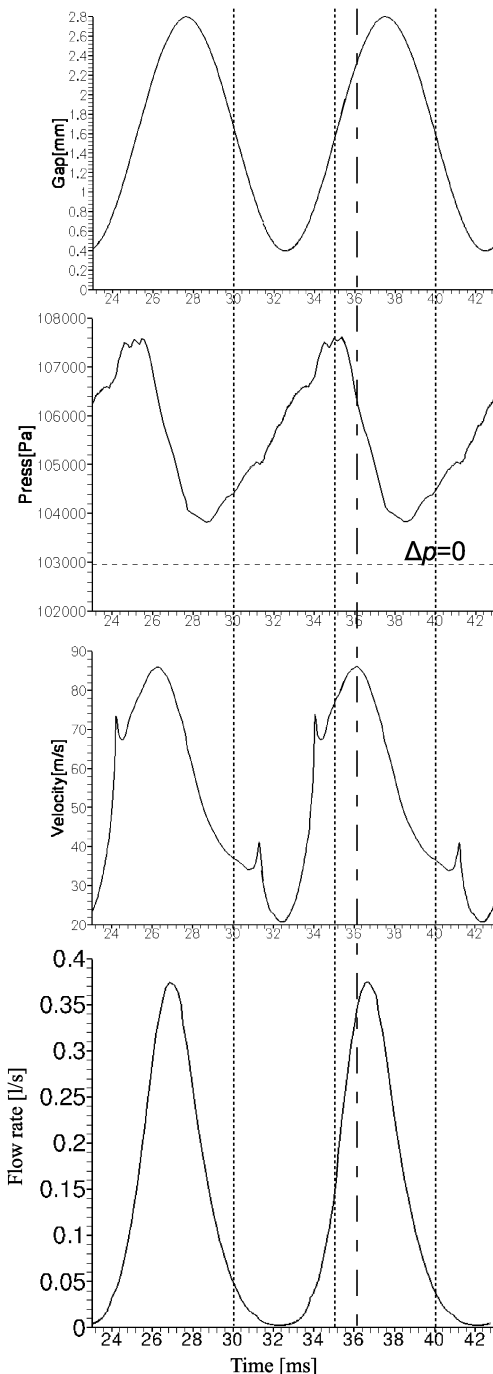


Fig.8: Periodic motion of the gap width (top graph), the pressure registered at the inlet (second graph), numerically simulated absolute airflow velocity at the narrowest cross-section on the channel axis (third graph) and the flow rate calculated in the narrowest channel cross-section (bottom graph); the data were computed in real time during the fourth oscillation period ($\hat{f} = 100$ Hz, $M_\infty = 0.012$, $Re_\infty = 5378$, $p_2 = 1/\kappa$, 450×100 cells)

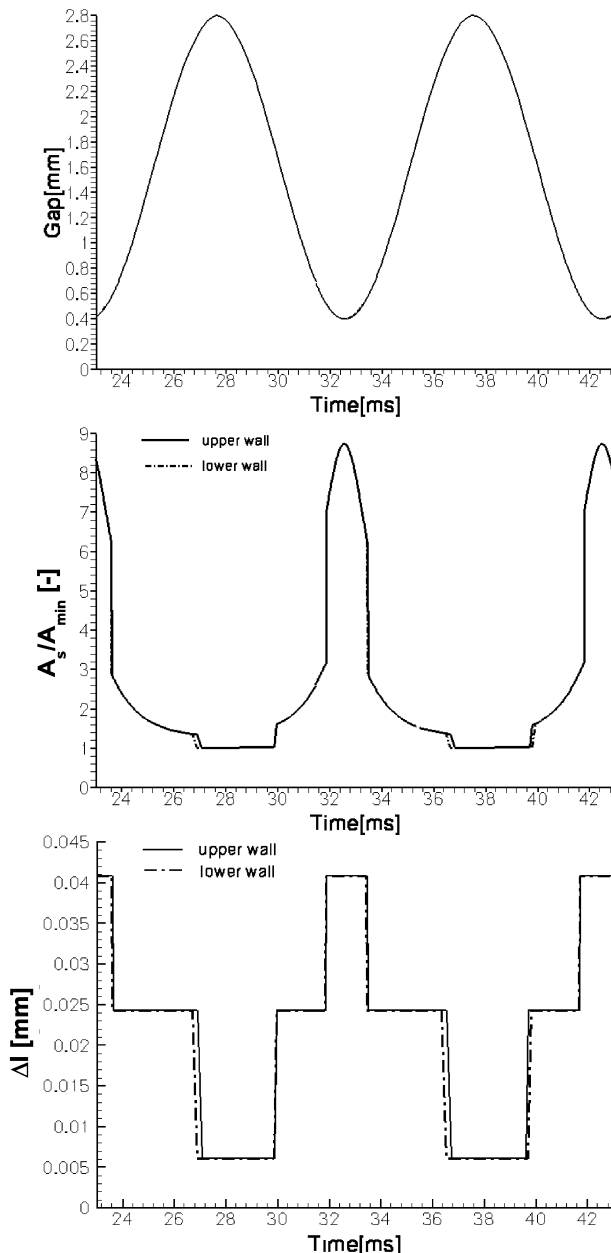


Fig.9: Periodic motion of the gap width (top graph), the separation point area ratio A_s/A_{\min} computed on the upper (solid line) and lower (dot-dashed line) walls of the channel during the fourth oscillation cycle (middle graph) and distance Δl of the separation point from narrowest channel cross-section point computed on the upper (solid line) and lower (dot-dashed line) walls (bottom graph) ($\hat{f} = 100$ Hz, $M_\infty = 0.012$, $Re_\infty = 5378$, $p_2 = 1/\kappa$, 450×100 cells)

Figure 9 shows the oscillation of gap width, the separation point area ratio A_s/A_{\min} computed on the upper and lower oscillating walls of the channel and distance Δl of the separation point from narrowest channel cross-section point on the upper and lower walls (see Figure 10). A_s and A_{\min} denote separation and minimum orifice areas, respectively, which are equivalent to orifice height for two-dimensional unit-depth simulation as shown in Figure 10. The minimum pressure on the wall is the criterion for the occurrence of the separation point. The values of the ratio vary from $A_s/A_{\min} = 1.02$, corresponding to the instant of maximum glottal gap width, to $A_s/A_{\min} = 8.74$, corresponding to the instant just after the gap opening phase started. The difference between upper and lower wall is very small. The wave form of separation ratio is skewed, the flow separation point moves on the vibrating wall differently in closing and opening phase, see bottom graph Δl in Figure 9. The jumps in the graph of the distance Δl are caused by changes in the flow field pattern in the model of the laryngeal cavity when pattern is changing from an axisymmetric to unsymmetric.

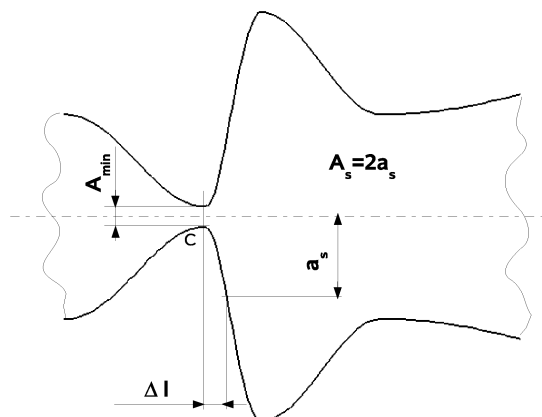


Fig.10: Measured widths A_s , A_{\min} and distance Δl

6. Discussion and conclusions

Special program code has been developed for numerical simulation of the airflow in a channel with vibrating walls for 2D unsteady viscous compressible fluid.

The results obtained for a simplified model of the glottal region are comparable with the results published in article [15], where the separation point and the glottal flow rate in a geometrically different channel were computed for a vibration frequency of 447Hz using FE model of the vocal folds and incompressible Navier-Stokes equations. In [15], the separation area ratio has been found out to be in the range $A_s/A_{\min} = 1.3-9.7$. The maximum flow rate and maximum glottal width were in phase and the minimum pressure lagged by approximately 1/10 of a period. It does not correspond to our findings, where maximum flow rate and pressure are delayed against the minimum gap. Comparing to our study this might have been caused by neglecting fluid compressibility and considering very high oscillation frequency not typical for normal voice. From the position of the sudden jumps in the ratio A_s/A_{\min} during the opening and closing phases (see Figure 9), it can be deduced that the flow separation point has been shifted stream-wise in the closing phase, as compared to the glottis opening phase.

The numerical solution in the channel showed large vortex structures developed in the supraglottal space moving slowly downstream and decaying gradually. It was possible to detect a ‘Coandă phenomenon’ in the computed flow field patterns. A similar generation of large-scale vortices, vortex convection and diffusion, jet flapping, and general flow patterns were experimentally obtained in physical models of the vocal folds by using PIV (Particle Image Velocimetry) method in [16], [17] and [10].

The results show that some numerical results of viscous flow in a symmetric channel using a symmetric grid and scheme can be non-symmetrical, depending on the geometry and the Reynolds number. This effect was observed also for laminar transonic flow computation, see [18]. The assumption of the axisymmetry solution for the axisymmetry channels (see [19]) excludes modeling the ‘Coandă’ effect and large vortex structures of the size comparable with the cross-section of the channel.

Acknowledgment

This contribution was partially supported by Research Plan MSM 6840770010 and grants of the MSM No. OC09019 and GA CR No. 201/08/0012.

References

- [1] Titze I.R.: Principles of Voice Production, National Centre for Voice and Speech, Iowa City, 2000, ISBN 0-87414-122-2
- [2] Horáček J., Šidlof P., Švec J.G.: Numerical simulation of self-oscillations of human vocal folds with Hertz model of impact forces, *Journal of fluids and structures*, 20: 853–869, 2005
- [3] Titze I.R.: The Myoelastic Aerodynamic Theory of Phonation, National Centre for Voice and Speech, Iowa City, 2006, ISBN 0-87414-122-2
- [4] Zöner S., Kalteenbacher M., Mattheus W., Brücker C.: Human phonation analysis by 3d aero-acoustic computation, In: Proceedings of the International Conference on Acoustic NAG/DAGA 2009, 1730–1732, Rotterdam, 2009
- [5] Pelorson X., Hirschberg A., van Hassel R.R., Wijands A.P.J., Auregan Y.: Theoretical and experimental study of quasisteady-flow separation within the glottis during phonation. Application to a modified two-mass model, *Journal of the Acoustical Society of America* 96: 3416–3431, 1994
- [6] Alipour F., Titze I.R.: Combined simulation of two-dimensional airflow and vocal fold vibration, In: P.J. Davis, N.H. Fletcher (Eds.), *Vocal Fold Physiology, Controlling Complexity and Chaos*, Singular, San Diego, 1996
- [7] De Vries M.P., Schutte H.K., Veldman A.E.P., Verkerke G.J.: Glottal flow through a two-mass model: Comparison of Navier-Stokes solutions with simplified models, *Journal of the Acoustical Society of America*, 111(4): 1847–1853, 2002
- [8] Rosa M.O., José Carlos Pereira: A contribution to simulating a three-dimensional larynx model using the finite element method, *Journal of the Acoustical Society of America* 114(5): 2893–2905, 2003
- [9] Fürst J., Janda M., Kozel K.: Finite volume solution of 2D and 3D Euler and Navier-Stokes equations, In: P. Neustupa, J. Penel (Eds.), *Mathematical fluid mechanics*, 173–194, Berlin, 2001
- [10] Horáček J., Šidlof P., Uruba V., Veselý J., Radolf V., Bula V.: PIV Measurement of Flow-Patterns in Human Vocal Tract Model, In: Proceedings of the International Conference on Acoustic NAG/DAGA 2009, 1737–1740, Rotterdam, 2009
- [11] Honzátko R., Horáček J., Kozel K.: Solution of inviscid incompressible flow over a vibrating profile, In: M. Beneš, M. Kimura, T. Nataki (Eds.), *COE Lecture notes*, 3: 26–32, Kyushu university, 2006, ISSN 1881-4042

- [12] Punčochářová P., Kozel K., Fürst J.: An unsteady numerical solution of viscous compressible flows in a channel, In: Program and Algorithms of Numerical Mathematics 13, 220–228, Math. Institute ASCR, 2006, ISBN 80-85823-54-3
- [13] Dvořák R., Kozel K.: Matematické modelování v aerodynamice, Vydavatelství ČVUT, Praha, 1996, ISBN 80-01-01541-6
- [14] Punčochářová P., Horáček J., Kozel K., Fürst J.: Numerical Simulation of Airflow through the Oscillating Glottis, In: Proceedings of the 5th international workshop MAVEBA 2007, 55–58, Firenze, Universita degli Studi, 2007, ISBN 978 88-8453-673-3
- [15] Decker G.Z., Thomson S.L.: Computational simulations of vocal folds vibration: Bernoulli versus Navier-Stokes, *Journal of Voice*, 21(3): 273–284, 2007
- [16] Šidllof P.: Fluid-structure interaction in human vocal folds, PhD thesis, 88, Charles University in Prague, Faculty of Mathematics and Physics, Prague, 2007
- [17] Neubauer J., Zhang Z., Miraghiae R., Berry D.: Coherent structures of the near field flow in self-oscillating physical model of the vocal folds, *Journal of the Acoustical Society of America*, 121(2): 1102–1118, 2007
- [18] Fořt J., Hůlek, Kozel K., Vavřincová M.: Remark on numerical simulation of 2D unsteady transonic flows, In: M. Napolitano & F. Sabetta (Eds.), Lecture notes in Physics, 414: 524–528, Springer-Verlag Berlin, Germany, 1993
- [19] Punčochářová P., Kozel K., Horáček J., Fürst J.: An Unsteady Numerical Solution of Viscous Compressible Flows in a Channel for Low Mach Numbers, *Journal of Computational and Applied Mechanics*, 8(2): 175–191, 2007, ISSN 1586-2070

Received in editor's office: October 14, 2009

Approved for publishing: May 17, 2010